Dental Materials Journal 2023; 42(3): 396–404

Development of a tooth movement model of root resorption during intrusive orthodontic treatment

Yue ZHOU[1], Aki NISHIURA[1], Hidetoshi MORIKUNI[1], Toru TSUJIBAYASHI[2], Yoshitomo HONDA[3] and Naoyuki MATSUMOTO[1]

[1] Department of Orthodontics, Osaka Dental University, 8-1 Kuzuhahanazono-cho, Hirakata, Osaka 573-1121, Japan
[2] Department of Physics, Osaka Dental University, 8-1 Kuzuhahanazono-cho, Hirakata, Osaka 573-1121, Japan
[3] Department of Oral Anatomy, Osaka Dental University, 8-1 Kuzuhahanazono-cho, Hirakata, Osaka 573-1121, Japan
Corresponding author, Aki NISHIURA; E-mail: nishiura@cc.osaka-dent.ac.jp

There is a high risk of external apical root resorption (EARR) following the application of intrusive orthodontic forces to the apical root. However, there is a lack of suitable animal models to study this phenomenon in depth. This study compared the usability of three different types of loops, namely, vertical helical loop, box loop, and L loop, for preparing a rat model of orthodontic tooth movement with invasive forces. Results showed a significant downward movement in the first molar of the rat after L loop placement for 14 days. Three-dimensional reconstructed images showed root resorption and length shortening on the apical root and decreased bone volume and trabecular thickness in the alveolar bone under compression. Histological staining revealed odontoclasts on the root resorption fossa. This study showed that orthodontic tooth movement using the L loop provides an effective experimental animal model of EARR.

Keywords: Orthodontics, Intrusion, EARR, L loop, Orthodontic tooth movement model

INTRODUCTION

External apical root resorption (EARR) is a phenomenon seen as a consequence of orthodontic treatment, often accompanied by the irreversible loss of apical root tissue[1]. In severe cases, root resorption shortens the root length, compromises masticatory support, and may even result in tooth loss[2]. Personal factors, such as genetics, systemic factors, degree of malocclusion, root morphology, duration of treatment, application of force, and amount of root movement during intraoral treatment, are risk factors for apical root resorption[3]. However, in clinical practice, it is difficult to identify the cause of EARR[4]. Although genetic and other factors are known to cause root resorption, there is limited information on other unrelated mechanisms, such as mechanical stimuli (mechanical stress).

In orthodontic treatment, tooth movement depends on force application from various directions depending on the treatment objective[5]. However, applying intrusive forces in orthodontic treatment often raises the risk of EARR[6]. In recent years, researchers have developed experimental animal models mimicking orthodontic tooth movement (OTM) for horizontal movement under mechanical stimulation, such as the model with a separator chain inserted between the first and second rat molars[7,8] and the closing coil spring model from the incisor to the first molar[9]. Most of the root resorption in these models occurred on the lateral sides of the root surface[10]. Furthermore, clinical studies on root resorption and restoration have focused on lateral resorption alone[11,12]. Few studies have examined apical root resorption models using rodents.

In orthodontic treatment, loops of geometric forms are fabricated with bendable wires (*e.g.*, stainless steel) to obtain the desired tooth movement[13]. Vertical helical loop[14], box loop[15], and L loop[16] are used for tooth movement in orthodontic treatment. These loops can return to its original state and exert force when the loop shape is squeezed[14-16]. It is widely used clinically in treating single or multiple teeth under pressure but may cause root resorption[17]. However, so far, no study has compared the usability of loops for preparing apical root resorption in the animal model.

Therefore, in this study, we fabricated three loops, namely, vertical helical loop, box loop, and L loop, to apply invasive forces through bent stainless steel wires used as invasive force excitation devices in orthodontic treatment and investigated whether they can be used in an experimental root resorption model.

MATERIALS AND METHODS

OTM model with loops for intrusive orthodontic force

Alginate impressions were taken from the arches of 15-week-old Sprague Dawley rats to prepare plaster casts of the maxillary molars. Based on the plaster model, we made a vertical helical loop, a box loop, and an L loop to fit the size of the rat molars (Fig. 1).

1) Preparing the vertical helical loop

To prepare the vertical helical loop, we used a stainless steel wire with a round (0.014 inches) cross-section (Ormco, Brea, CA, USA) that was bent using light wire pliers commonly used in clinical treatment (Fig. 2A). Part of the wire was fixed to the M2 and M3 occlusal surfaces: ab (3.0 mm); vertical helical loop had two vertical sections: xe and cg (2.0 mm), and a 1.0 mm radius

Received Nov 1, 2022: Accepted Dec 7, 2022
doi:10.4012/dmj.2022-247 JOI JST.JSTAGE/dmj/2022-247

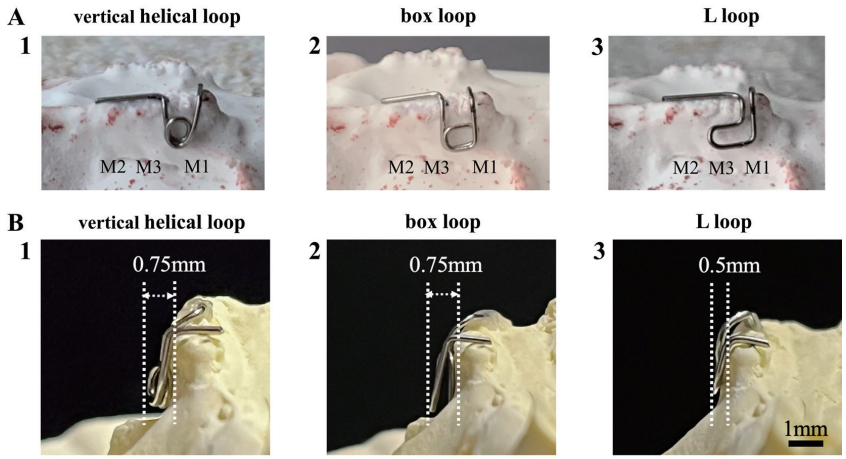

Fig. 1 Three types of bent orthodontic loops based on the rat molar model.
(A) Three types loops, namely, vertical helical loop, box loop, and L loop. (B) Comparison of the buccal side thicknesses of the three loops. Scale bar=1 mm. M1: first molar; M2: second molar; M3: third molar

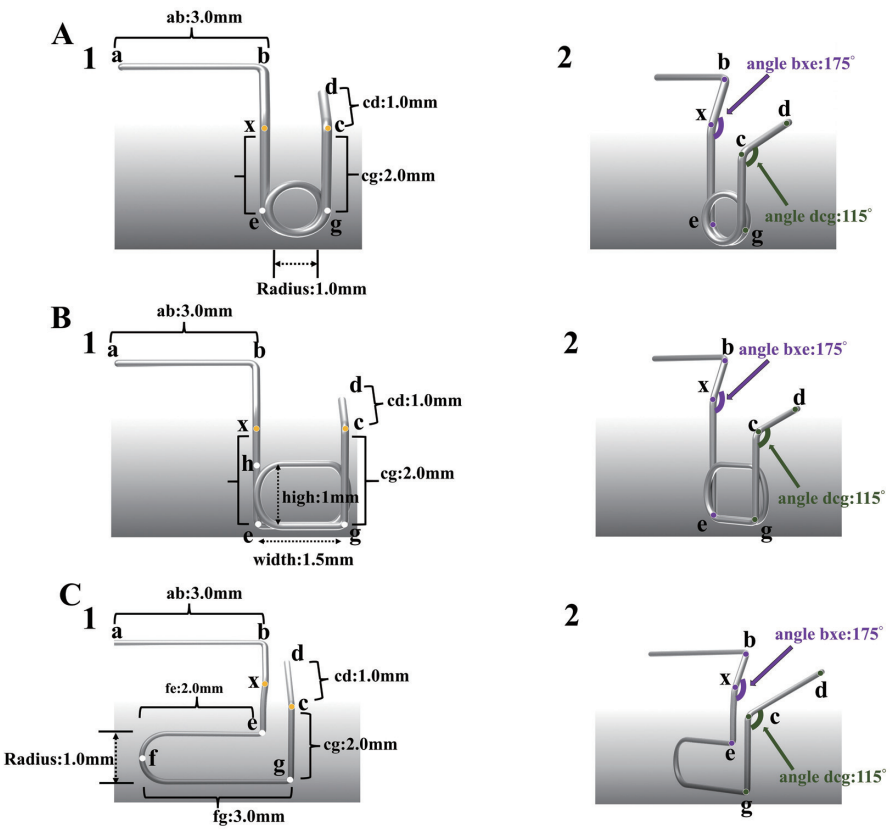

Fig. 2 Three loops OTM model for intrusive orthodontic force.
(A) vertical helical loop, (B) box loop, (C) L loop

of the helical sections. The other part of the wire was fixed to the M1 occlusal plane: cd (1.0 mm) (Fig. 2A.1). To avoid buccal gingival tissue, ab formed a 175° angle with the vertical helical part (angle: bxe). To control the vertical movement of M1, cd formed a 115° angle with cg (angle: dcg) (Fig. 2A.2). To activate the vertical helical loop curve, ab formed a 1.0 mm height step with cd (Fig. 2A.1). The thickness of the buccal side of the loop tissue was 0.75 mm (Fig. 1B.1).

2) Preparing the box loop
The same material (0.014 inches round stainless steel

wire) was used to make box loops (Fig. 2B). Part of the wire was fixed to the M2 and M3 occlusal surfaces: ab (3.0 mm). The box loop had two vertical sections: xe and cg (2.0 mm); the width of the bottom box: eg (1.5 mm), and the height of the bottom box: eh (1.0 mm) (Fig. 2B.1). As with the vertical helical loop, ab formed a 175° angle with the box (angle: bxe). To control the vertical movement of M1, cd formed a 115° angle with cg (angle: dcg) (Fig. 2B.2). To activate the box loop curve, ab formed a 1.0 mm height step with cd (Fig. 2B.1). The thickness of the buccal side of the loop tissue was 0.75 mm (Fig. 1B.2).

3) Preparing for the L loop

For preparing the L loop, the same material (stainless steel 0.014 inches round wire) was used to make L loops. L loops were bent according to the specifications shown in Fig. 2C. The part of wire fixed to M2 and M3 occlusal surfaces: ab (3.0 mm); L loop's upper portion: fe (2.0 mm); L loop's lower portion: fg (3.0 mm); L loop's vertical portion: cg (2.0 mm); the part of wire fixed to the M1 occlusal plane: cd (1.0 mm) (Fig. 2C.1); to avoid buccal gingival tissue, ab formed a 175° angle with the L shaped curved part (angle: bxe); to control the vertical movement of M1, cd formed a 115° angle with cg (angle: dcg) (Fig. 2C.2). To activate L loop curve, ab formed a 1.0 mm height step with cd (Figs. 2C and Fig. 3A). The thickness of the buccal side of the loop tissue was 0.5 mm (Fig. 1B.3).

The ab end of each loop was vertically pressed to about 1.0 mm, and compression tests were performed using a Universal Material Testing Force measuring device. Each loop was measured thrice by the same experimenter.

Universal material testing for the three loops

The wires used in the experiments were all bent by the same experimenter with uniform standards.

1) First, the maxillary bone model of 15-week-old rats were encased in a super hard plaster, exposing the molar portion. A glass plate was used to test and ensure the level of the plaster base to ensure the instrument

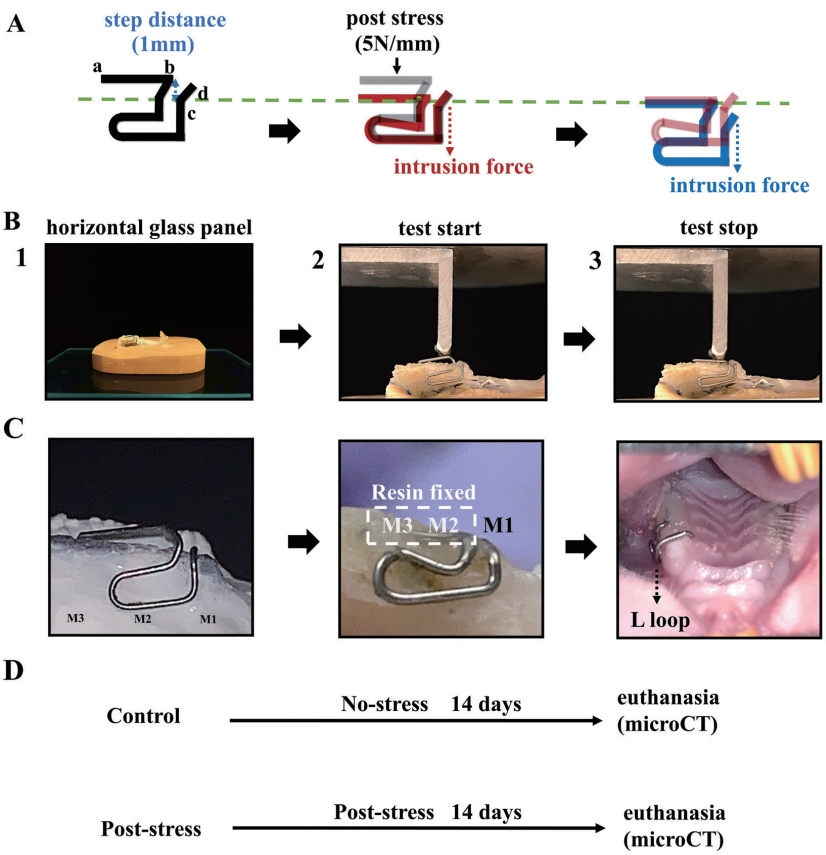

Fig. 3 Universal material testing and animal experiment.
(A) The represent schematic images to induce intrusion force using L loop. To activate the L loop curve, ab formed a 1.0 mm height step with cd (the translucent line segment represents the shape of the wire before the compression deformation). (B) Macroscopic images of the universal material testing experiments. (B1) Glass plate for checking the level of the plaster model base. (B2) The loop state when the universal material testing experimental device starts testing. (B3) The loop state when the universal material testing experimental device stops testing. (C) Macroscopic Images of L loop in a rat molar plaster model and in oral cavity. (D) Workflow of animal experiments.

stability of the model during force measurement (Fig. 3B.1). The loop was mounted on the left molars of the rats, and a small amount of resin was used to secure the ab portion of the loop to the M1 occlusal surface (Fig. 3B.1 and 2). The loops were mounted on the M1, M2, and M3 occlusal surfaces of the left molars of the rats in the same manner as in the animal experiments.

2) Starting from the probe part of the force gauge nearly touching the ab section of the wire (Fig. 2B.2), the force was measured by pressing down the wire at a speed of 1 mm/min at a constant rate and stopping the force measurement when the ab section of the wire touched the M2 and M3 occlusal surfaces (Fig. 2B.3). We chose the data when the force measurement was finally stopped as the activation force (N) and the loop press-down distance (mm) of the wire.

3) The same experimenter performed the same method for three force measurement experiments of each loop.

Animal experiment

In the animal experiment, 15-week-old Sprague Dawley rats weighing 400 g were assigned to the control (without orthodontic appliances) and the post-stress groups (with vertical helical loops, box loops, L loops, on the buccal side of the maxillary left molars M1, M2, M3) (four rats in each group; Figs. 3C and D). All rats were housed in 12 h alternating light and dark environment. To prevent mastication movements from interfering with the experimental setup, the rats were fed soft paste feeds. The occlusal surfaces of the non-experimental contralateral molars were padded with 1 mm resin to prevent initial contact interference on the experimental side occlusion. Both groups were euthanized after 14 days and perfusion-fixed in 10% neutral formalin. The animal experiment was approved by the local ethics committee of Osaka Dental University, and the policy was strictly observed (approval number: 20-03007).

Micro-CT analysis

Dissected maxillary bones were scanned using microcomputed tomography (SkyScan1275, Bruker, Billerica, MA, USA) at 85 kV, 65 μA, 1,925×1,725 resolution. Post-scan data were reconstructed in 3D using SkyScan™ CT Analyzer software (version 1.17.7.2). The distance of intrusion at 14 day was quantified using the μCT data and Image J (version: 2.1.0, U.S. National Institutes of Health, Bethesda, MD, USA). The buccal margin of the crown of the left molars M2 and M3 was used as the baseline, and the vertical distance from the buccal cusp of the first molar to this baseline was measured. A 30-layer CT image of the root apex of the buccal central root of the first molar was selected for root mineral density (RMD) measurement. A 200 μm^3 cube of alveolar bone below the buccal central root was selected for calculating bone volume fraction (BV/TV), trabecular number (Tb.N), trabecular thickness (Tb/Th), and trabecular separation (Tb/Sp) of the alveolar bone on the compression side. The DICOM data taken were reconstructed in Mimics (13.1 software Materialise, Leuven, Belgium). The central root was separately rendered to observe apical resorption morphology.

Histological staining

Maxillary bones were fixed in a 10% neutral formalin solution for 48 h. EDTA neutral demineralization solution B (Cat No. LEP2494, Fujifilm, Osaka, Japan) was used to demineralize at 4 degrees. The demineralization solution was changed every other day. After 2 weeks of continuous demineralization, dehydration was performed using a sucrose gradient of 10%, 20%, and 30%. Samples were freeze-embedded according to the Kawamoto method, and frozen sections of 10 μm thickness were prepared on a freezing microtome (Leica CM3050S, Leica Biosystems, Richmond, IL, USA). Frozen sections were stained with hematoxylin-eosin (H-E) using standard techniques. The tartrate-resistant acid phosphatase (TRAP) staining was performed according to the staining protocol provided by the manufacturer using a TRAP/ALP Stain Kit (Cat No. 294-67001, Fujifilm). Images were captured using an HS All-in-One Fluorescence Microscope BZ-9000 (Keyence, Osaka, Japan).

Statistical analysis

All data were statistically analyzed using Prism 8 (GraphPad Software, San Diego, CA, USA). Student's *t*-test was performed for comparison between the two groups. $p<0.05$ was considered statistically significant.

RESULTS

Before the animal experiments began, we selected three types of loops and fabricated the devices as designed because we were unaware of which loop was suitable. We measured the maximum force required to press down the ab part of the loop to the M2 and M3 occlusal planes (Table 1); in the meanwhile, we also measured the distance to be moved when pressing down the ab part of the loop to the M2 and M3 occlusal planes (Table 2). We loaded each type of loop on the left molar of four rats and observed loop drop-down, loop retention, CT images, and the number of rats showing the occurrence of EARR in TRAP staining data (Table 3). The results are presented in the following section.

The results of the vertical helical and box loops show an average maximum experimental force of 2.8 N and 1.75 N, respectively. The average maximum test force of the L loops was 4.97 N (Table 1). While pressing down the ab part of the loop to the M2 and M3 occlusal surfaces, the vertical helical and box loops' ab parts moved approximately 0.98 mm and 0.90 mm, respectively, and the L loop moved approximately 1.08 mm on average (Table 2). Although we prepared three different loops, the vertical helical and box loops had different degrees of dropout during loop loading. Among the four rats loaded with loops, only one rat with the vertical helical loop developed EARR, whereas none with the box-loop developed EARR. The L loop performed more favorably than the vertical helical and box loops, with no loop dropout, and all four rats with the L loop developed

Table 1 Universal Material Testing Force for three loops

	vertical helical loop Force (N)	box loop Force (N)	L loop Force (N)
	2.7	2.0	4.8
Rat 1	2.3	1.9	5.1
	2.5	1.8	4.9
	3.0	2.1	5.0
Rat 2	3.1	2.6	5.0
	2.9	2.7	5.0
	2.6	1.3	5.0
Rat 3	2.8	1.0	5.0
	2.9	1.4	5.1
	3.0	1.6	5.0
Rat 4	2.9	1.2	5.1
	3.0	1.4	4.9
Mean (SD)	2.80 (0.24)	1.75 (0.53)	4.97 (0.086)

SD (Standard Deviation)

Table 2 Loop press-down movement distance for three loops

	vertical helical loop distance (mm)	box loop distance (mm)	L loop distance (mm)
	0.9	0.9	0.8
Rat 1	1.0	0.8	1.1
	0.9	0.8	1.0
	1.1	0.7	1.2
Rat 2	1.1	1.0	1.2
	1.0	1.1	1.0
	0.8	1.1	1.1
Rat 3	1.0	0.7	1.0
	1.0	1.1	1.3
	1.0	0.9	1.3
Rat 4	0.8	0.7	1.0
	1.1	0.9	1.0
Mean (SD)	0.98 (0.11)	0.90 (0.15)	1.08 (0.14)

SD (Standard Deviation)

Table 3 Loop loading and root resorption ratio of three loops

	loop loading rats	loop dropout rats	loop maintaining rats	EARR rats Ratio (CT)	EARR rats Ratio (TRAP)
vertical helical loop	4	2	2	1/4	1/4
box loop	4	2	2	0/4	0/4
L loop	4	0	4	4/4	4/4

EARR rats ratio: The number of four experimental rats loaded with loops in which EARR occurred.

EARR (Table 3). Additionally, the vertical helical and box loops did not show good instrument stability or reproducibility in universal material testing and animal experiments. Therefore, we focused on the effectiveness of the L loop in the subsequent experiments.

Micro-CT reconstruction images showed that M1 in the experimental group after L loop loading was significantly displaced downward after 14 days compared to the control group (Fig. 4). High resolution sagittal images showed that at the 14-day, L loop wearing group

had serrated resorption at the apical part, an upward-facing, irregularly shaped resorptive fossa (white arrowheads indicate the root resorption fossa) (Fig. 5A). For further observation, a Mimics reconstruction of the CT data was performed to visualize the irregular shortening of the central root tip from the normal

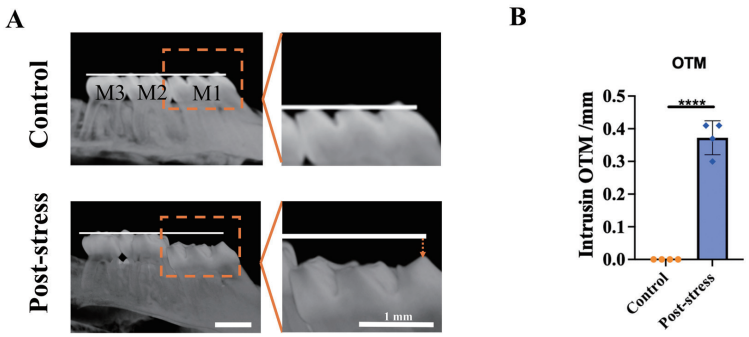

Fig. 4 The intrusive OTM of the first molar of the rat after fitting the L loop.
(A) Reconstructed micro-CT images of rat maxillary left molars. White lines indicate OTM measurement reference lines. Orange arrow indicates the M1's OTM distance. (B) Statistical quantitative analysis of intrusive OTM distances. ****p<0.0001, Scale bar=1 mm

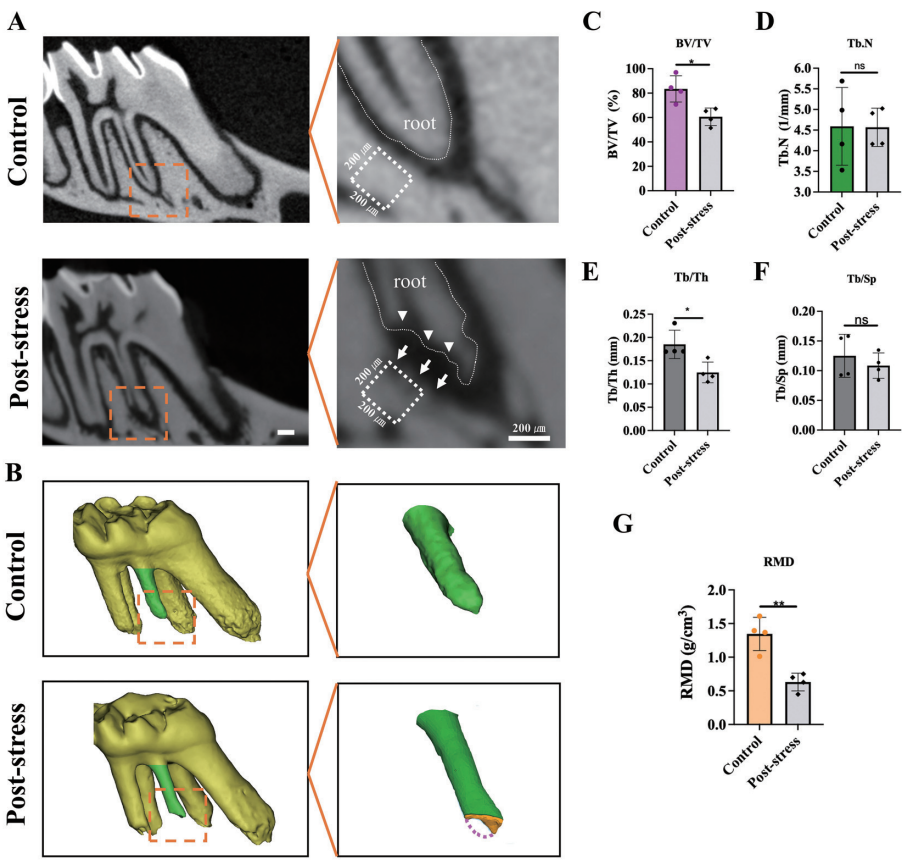

Fig. 5 Micro-CT's three-dimensional reconstructions of the M1 buccal central root.
(A) Sagittal image of the buccal lateral central root. White arrow indicates the hypodense images of the alveolar bone. White arrowhead indicates the root resorption fossa. (B) The reconstructed images of the central root using Mimics software. The orange section indicates the cross-section of root tip uptake. The pink dashed line indicates the original shape of the root tip in the experimental group. (C) The 200 μm^3 volume of alveolar bone below the central root apical: Bone volume fraction (BV/TV). (D) Trabecular number (Tb.N). (E) Mean trabecular thickness (Tb.Th). (F) Trabecular separation (Tb.Sp). (G) RMD at the central root apical. *p<0.05, **p<0.01, ns: not significant. Scale bar=200 μm

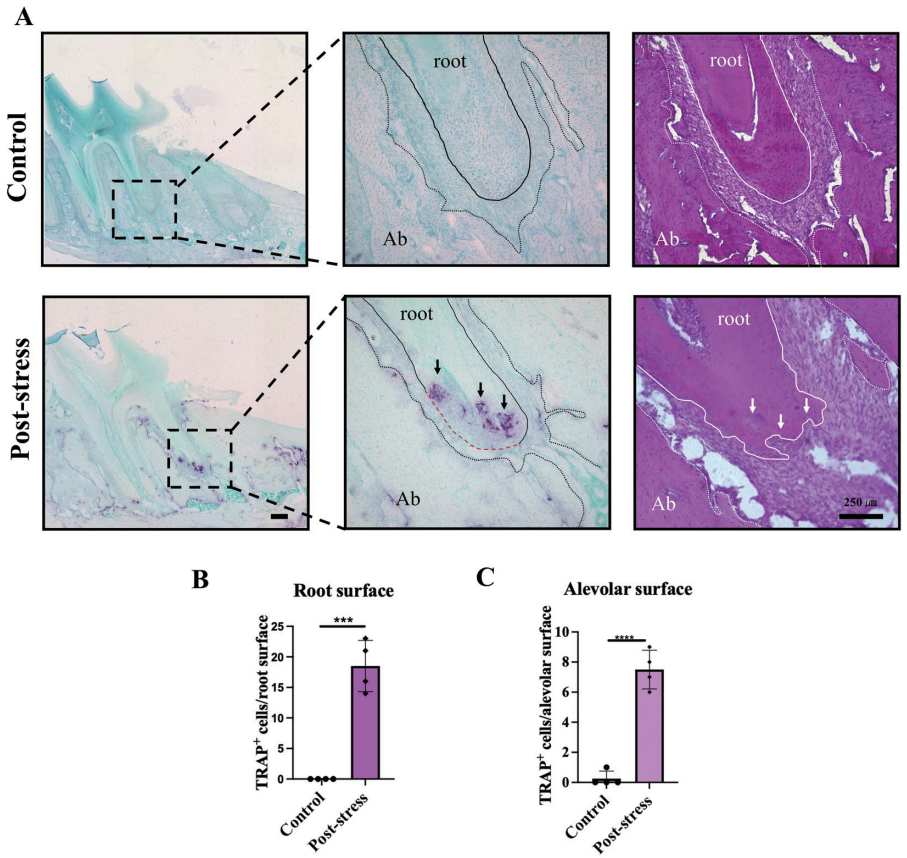

Fig. 6 Histological staining of the central apical root.
(A) TRAP staining and H-E staining of the central root apical. Black arrows and white arrows represent root resorption fossa. (B) Statistical analysis of the number of TRAP-positive cells on the root surface. The red dashed line indicates the original shape of the apical root. (C) Statistical analysis of the number of TRAP-positive cells on the alveolar bone surface. ***p<0.001, Ab: Alveolar bone, Scale bar=250 μm

rounded curve (Fig. 5B). Quantitative CT analysis revealed that BV/TV and Tb/Th of the alveolar bone on the compression side decreased (Figs. 5C and E). The low radiopacity of the alveolar bone also indicated bone resorption below the central root (Fig. 5A; white arrow). Meanwhile, Tb.N and Tb/Sp did not change significantly (Figs. 5D and F). In rats loaded with L loop for 14 days, there was also a significant decrease in RMD in the root portion of the central root (Fig. 5G).

TRAP staining and its quantitative data showed numerous TRAP positive cells on the irregular resorption fossa of the root surface at the central root tip under the OTM (black arrows) (Figs. 6A and B). H-E staining of the same area also confirmed the presence of root resorption fossa (white arrows). TRAP positive cells also appeared on the alveolar bone surface (Figs. 6A and C).

DISCUSSION

In the present study, to simulate intrusive force-induced EARR, we prepared three different types of loops used in clinical orthodontic treatment. The L loop showed a higher testing force than the vertical helical and box loops during the force measurement for a displacement of approximately 1.0 mm. In addition, all four rats with the L loop showed a higher root resorption rate than those with the other two loops (Table. 3). In contrast to the first two loops, the L loop loading successfully exhibited higher instrument stability in producing root resorption within 14 days.

Although root resorption and repair are known to occur laterally during orthodontic treatment, the mechanism of root resorption is fully unknown[18]. Some studies have shown that intrusive forces cause approximately four times more root resorption than extrusive forces[19]. Furthermore, intrusion increases the risk of apical root resorption[20], although the reasons for this phenomenon remain largely unknown.

Commonly used metal materials for orthodontic wires are stainless steel, nickel titanium, and titanium molybdenum[21]. Since the introduction into orthodontic treatment, stainless steel wires are widely used for their malleability, biocompatibility, environmental stability, hardness, elasticity, low cost, and low resistance to tooth movement[22]. The stainless steel wire has a higher modulus of elasticity compared to the nickel titanium

and titanium molybdenum alloys. The greater modulus of elasticity means that more force is required to bend the stainless steel wire[23] . Nickel titanium alloys cannot be used to design loops because they are not inherently bendable metals. For that reason, stainless steel can bend and adjust the opportunity force you want to add by adjusting the shape of the loop and the length of the wire, while the other two types of wires have difficulty doing so. The high modulus of elasticity of stainless steel is such that moderately low orthodontic forces are sustained during tooth movement with loops[24]. Taking advantage of this property of stainless steel, we designed the L loop to deform the L shaped curved part by pushing the end of the ab wire to the M2, M3 occlusal surface, and the force generated by the wire moved the tooth downward through the return of the shape (Figs. 3A–C).

In this study, although we prepared three different loops, the vertical helical and box loops had varying degrees of dropout during the loop loading process (Table. 3). Root resorption occurred in only one of the four rats with the vertical helical loop and in none of the four rats with the box loop (Table 3). This may be because the buccal thickness of these two loops is greater than that of the L loop (Fig. 1B), and the movement of the buccal muscle tissue in the rats hinders the instrument stability of the loops.

During the preparation of the loops, although we measured the step distance between the ab and cd parts of the loop with Vernier calipers to be 1.0 mm, a loss of height was noted during the actual measurement, which was also reflected in the loop press-down movement distance in the universal testing force experiment (Table 3). The actual displacement measured using the universal force gauge is the distance from when the gauge joint first touches the ab section of the wire to when the wire is pressed down to just touch the M2 and M3 occlusal surfaces (Fig. 3B.2 and 3). However, when we operate the universal testing machine, the device made of round steel wire is pushed, which sometimes causes the device to move slightly, thereby generating a loss of height; this may explain the actual displacement of the wire of approximately 0.8–1.3 mm. On the other hand, because of the narrow space in the rat mouth, a small loss of actual depression height was noted during the animal experiments. This can be improved in subsequent experiments.

In our experiments, we designed the buccal angle of the L loop so that the angle between the occlusal surface and the buccal side was 175° to avoid gingival compression in rats (Fig. 2C.2). Previous mechanical analysis experiments of loop showed that the pressure drop force generated at the ab end during loop deformation was transferred to the cd (M1 occlusal plane) with an almost constant pressure drop force[16]. However, in this study, the cd portion of the L loop was set in the buccal-lingual direction of the M1 occlusal plane so that the force applied to point d (the wire end) was weaker compared to point c. Therefore, the cheek side had more pressure drop, the lingual side had less pressure drop, and the teeth moved as if tilted. To avoid the tilting of M1 in the buccal-lingual direction, the angle of the cd portion where the vertical portion of the cg of the loop contacts the occlusal surface of M1 was made small (115°) to ensure the horizontal descent of M1 (Fig. 2C.2). In clinical treatment, continuous and heavy orthodontic forces are more likely to cause EARR[3,25,26]. In a study by Han *et al.*[19], the application of a heavy 100 cN intrusive force to human first premolars for 8 weeks resulted in EARR in almost all patients. In our study, the intrusive force during L loop wearing was adjusted to 5 N (corresponding to approximately 500 cN; Table. 1). Force application for 14 days resulted in clear vertical downward movement of M1 in rats (Fig. 4A). When clinical EARR occurs, patients often experience significant and irreversible shortening of the root length[27]. This finding was corroborated by micro-CT, which is similar to the 3D reconstructed images of central roots with shortened root lengths (Figs. 5A and B). Our experimental results show that significant external resorption of the root apex occurs in rats under continuous heavy intrusive force.

Bone remodeling is essential for OTM, which distributes mechanical stress to the periodontal ligament as force is applied to the root, promoting bone resorption on the compression side and bone renewal on the tension side[28,29]. After 14 days of L loop placement, a decrease in BV/TV and Tb/Th occurred in 200 cubic microns of alveolar bone below the central root compression side (Fig. 5A). The low radiopacity of the alveolar bone also indicates bone resorption below the central root (Fig. 5A; white arrow). Intriguingly, a significant decrease in the trabecular thickness (Tb/Th) was observed on day 14 after L loop loading (Fig. 5E). However, there was no significant change in the number of trabecular bones (Tb.N) (Fig. 5D). The results are consistent with the findings of Ru and colleagues[30], who suggest that resorption occurs on the trabecular bone surface of the alveolar bone beneath the compression side.

In this study, we produced and compared the availability, instrument stability, and repeatability of three different types of loops-vertical helical loop, box loop, and L loop. Furthermore, we focused on the effectiveness of the L loop as an OTM model of EARR under orthodontic invasive forces. The subject molar M1 successfully moved in pressure after 14 days of L loop application. The apex of the mesial buccal root showed significant resorption and shortening. However, different forces, time, wire diameter, and material may alter the outcomes. Other experimental conditions may offer additional findings. However, the series of our results should provide valuable insights for using orthodontic devices to prepare usable animal models causing EARR.

CONCLUSION

In the present study, we demonstrated that, 14 days after placing the L loop, intrusive orthodontic treatment can be applied in the rat's M1 molars. The root

resorption fossa and TRAP-positive cells were identified at the apical of the M1's central root. Micro-CT showed a shortened length of the central root; RMD of the roots and underlying alveolar bone volumes decreased. Additionally, the trabecular bone morphology of the alveolar bone was altered. These results suggest that the L loop enables the application of intrusive force to the tooth and is one of the effective methods for preparing experimental animal models for EARR at the apical root due to pressure drop.

ACKNOWLEDGMENTS

We thank Niuxin Yang, Wenqi Deng, Liji Chen, Chuyi Luo, Yosuke Miyaji, Hiroshi Matoba (Department of Orthodontics, Osaka Dental University) and Ye Zhang, Yuzhu Sun (Department of Biomaterials, Osaka Dental University) for the insights on animal experiments, and Jingzhao Lyu (Department of Orthodontics, Fudan University) for support and guidance on orthodontics.

REFERENCES

1) Topkara A, Karaman AI, Kau CH. Apical root resorption caused by orthodontic forces: A brief review and a long-term observation. Eur J Dent 2012; 6: 445-453.
2) Pinheiro LHM, Guimarães LS, Antunes LS, Küchler EC, Kirschneck C, Antunes LAA. Genetic variation involved in the risk to external apical root resorption in orthodontic patients: A systematic review. Clin Oral Investig 2021; 25: 5613-5627.
3) Weltman B, Vig KW, Fields HW, Shanker S, Kaizar EE. Root resorption associated with orthodontic tooth movement: A systematic review. Am J Orthod Dentofacial Orthop 2010; 137: 462-476; discussion 12A.
4) Elhaddaoui R, Benyahia H, Azeroual MF, Zaoui F, Razine R, Bahije L. Resorption of maxillary incisors after orthodontic treatment —Clinical study of risk factors. Int Orthod 2016; 14: 48-64.
5) Jiang T, Wu RY, Wang JK, Wang HH, Tang GH. Clear aligners for maxillary anterior en masse retraction: A 3D finite element study. Sci Rep 2020; 10: 10156.
6) Dermaut LR, De Munck A. Apical root resorption of upper incisors caused by intrusive tooth movement: A radiographic study. Am J Orthod Dentofacial Orthop 1986; 90: 321-326.
7) Nagaie M, Nishiura A, Honda Y, Fujiwara S, Matsumoto N. A comprehensive mixture of tobacco smoke components retards orthodontic tooth movement via the inhibition of osteoclastogenesis in a rat model. Int J Mol Sci 2014; 15: 18610-18622.
8) Matoba H, Nishiura A, Honda Y, Fujiwara S, Matsumoto N. Smoking cessation rescues tooth movement delays caused by tobacco smoke components. Orthod Waves 2021; 80: 17-22.
9) Burrow SJ, Sammon PJ, Tuncay OC. Effects of diazepam on orthodontic tooth movement and alveolar bone cAMP levels in cats. Am J Orthod Dentofacial Orthop 1986; 90: 102-105.
10) Yang F, Wang XX, Ma D, Cui Q, Zheng H, Liu XC, *et al.* Effects of triptolide on tooth movement and root resorption in rats. Drug Des Devel Ther 2019; 13: 3963-3975.
11) Cheng LL, Türk T, Elekdağ-Türk S, Jones AS, Yu Y, Darendeliler MA. Repair of root resorption 4 and 8 weeks after application of continuous light and heavy forces on premolars for 4 weeks: A histology study. Am J Orthod Dentofacial Orthop 2010; 138: 727-734.
12) Dindaroğlu F, Doğan S. Evaluation and comparison of root resorption between tooth-borne and tooth-tissue borne rapid maxillary expansion appliances: A CBCT study. Angle Orthod 2016; 86: 46-52.
13) Burstone CJ. The segmented arch approach to space closure. Am J Orthod 1982; 82: 361-378.
14) Sudhakar SS, Shrinivasa KA, Shetty P, Antony G, Shaji MS. A comprehensive review on loops in orthodontics. IP Indian J Orthod Dentofac Res 2021; 7: 191-207.
15) Martins RP, Shintcovsk RL, Shintcovsk LK, Viecilli R, Martins LP. Second molar intrusion: Continuous arch or loop mechanics? Am J Orthod Dentofacial Orthop 2018; 154: 629-638.
16) Techalertpaisarn P, Versluis A. How do mechanical responses at closing loop ends vary when loop position changes? A systematic analysis of vertical, T-, and L-loops. Oral Sci Int 2013; 10: 58-64.
17) Motokawa M, Sasamoto T, Kaku M, Kawata T, Matsuda Y, Terao A, *et al.* Association between root resorption incident to orthodontic treatment and treatment factors. Eur J Orthod 2012; 34: 350-356.
18) Lopatiene K, Dumbravaite A. Risk factors of root resorption after orthodontic treatment. Stomatologija 2008; 10: 89-95.
19) Han G, Huang S, Von den Hoff JW, Zeng X, Kuijpers-Jagtman AM. Root resorption after orthodontic intrusion and extrusion: An intraindividual study. Angle Orthod 2005; 75: 912-918.
20) Costopoulos G, Nanda R. An evaluation of root resorption incident to orthodontic intrusion. Am J Orthod Dentofacial Orthop 1996; 109: 543-548.
21) Castro SM, Ponces MJ, Lopes JD, Vasconcelos M, Pollmann MCF. Orthodontic wires and its corrosion —The specific case of stainless steel and beta-titanium. J Dent Sci 2015; 10: 1-7.
22) Kapila S, Sachdeva R. Mechanical properties and clinical applications of orthodontic wires. Am J Orthod Dentofacial Orthop 1989; 96: 100-109.
23) Drake SR, Wayne DM, Powers JM, Asgar K. Mechanical properties of orthodontic wires in tension, bending, and torsion. Am J Orthod 1982; 82: 206-210.
24) Zheng LW, Wang JY, Qing Yu R. Biomaterials in Dentistry. In: Narayan R, editor. Encyclopedia of Biomedical Engineering. Oxford: Elsevier; 2019. p. 278-288.
25) Harris DA, Jones AS, Darendeliler MA. Physical properties of root cementum: part 8. Volumetric analysis of root resorption craters after application of controlled intrusive light and heavy orthodontic forces: A microcomputed tomography scan study. Am J Orthod Dentofacial Orthop 2006; 130: 639-647.
26) Barbagallo LJ, Jones AS, Petocz P, Darendeliler MA. Physical properties of root cementum: Part 10. Comparison of the effects of invisible removable thermoplastic appliances with light and heavy orthodontic forces on premolar cementum. A microcomputed-tomography study. Am J Orthod Dentofacial Orthop 2008; 133: 218-227.
27) Marques LS, Ramos-Jorge ML, Rey AC, Armond MC, Ruellas AC. Severe root resorption in orthodontic patients treated with the edgewise method: Prevalence and predictive factors. Am J Orthod Dentofacial Orthop 2010; 137: 384-388.
28) Sun Q, Lu W, Zhang Y, Peng L, Chen S, Han B. Morphological changes of the anterior alveolar bone due to retraction of anterior teeth: A retrospective study. Head Face Med 2021; 17: 30.
29) de Sousa FRN, de Sousa Ferreira VC, da Silva Martins C, Dantas HV, de Sousa FB, Girão-Carmona VCC, *et al.* The effect of high concentration of zoledronic acid on tooth induced movement and its repercussion on root, periodontal ligament and alveolar bone tissues in rats. Sci Rep 2021; 11: 7672.
30) Ru N, Liu SS, Zhuang L, Li S, Bai Y. In vivo microcomputed tomography evaluation of rat alveolar bone and root resorption during orthodontic tooth movement. Angle Orthod 2013; 83: 402-409.